JACS
JOURNAL OF THE AMERICAN CHEMICAL SOCIETY
Article
pubs.acs.org/JACS

Mechanism of Protection of Catalysts Supported in Redox Hydrogel Films

Vincent Fourmond,[†] Stefanie Stapf,[‡,§] Huaiguang Li,[‡] Darren Buesen,[‡] James Birrell,[∥] Olaf Rüdiger,[∥] Wolfgang Lubitz,[∥] Wolfgang Schuhmann,[§] Nicolas Plumeré,*[,‡] and Christophe Léger*[,†]

[†]Laboratoire de Bioénergétique et Ingénierie des Protéines, Aix Marseille Université, CNRS, BIP UMR 7281, 13402 Marseille, France
[‡]Center for Electrochemical Sciences-Molecular Nanostructures, and [§]Analytical Chemistry, Center for Electrochemical Sciences (CES), Elektroanalytik & Sensorik, Ruhr-Universität Bochum, Universitätsstr 150, D-44780 Bochum, Germany
[∥]Max-Planck-Institut für Chemische Energiekonversion, Stiftstr 34-36, 45470 Mülheim an der Ruhr, Germany

Supporting Information

ABSTRACT: The use of synthetic inorganic complexes as supported catalysts is a key route in energy production and in industrial synthesis. However, their intrinsic oxygen sensitivity is sometimes an issue. Some of us have recently demonstrated that hydrogenases, the fragile but very efficient biological catalysts of H_2 oxidation, can be protected from O_2 damage upon integration into a film of a specifically designed redox polymer. Catalytic oxidation of H_2 produces electrons which reduce oxygen near the film/solution interface, thus providing a self-activated protection from oxygen [Plumeré et al., *Nat Chem.* **2014**, *6*, 822−827]. Here, we rationalize this protection mechanism by examining the time-dependent distribution of species in the hydrogenase/polymer film, using measured or estimated values of all relevant parameters and the numerical and analytical solutions of a realistic reaction-diffusion scheme. Our investigation sets the stage for optimizing the design of hydrogenase-polymer films, and for expanding this strategy to other fragile catalysts.

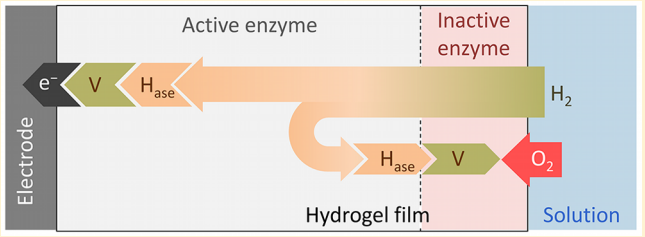

1. INTRODUCTION

Climate change and fossil fuel depletion are two major global societal challenges. Worldwide research and development efforts target the production and use of "green" energy carriers such as hydrogen and other small organic molecules. Currently, the catalysts for technological energy conversion are based on rare and expensive metals such as platinum, but it has been proposed that metalloenzymes or synthetic molecular catalysts based on abundant metals could be used instead. Enzymes are particularly attractive as model systems: those that reversibly convert either H^+ and H_2 (hydrogenases) use inorganic cofactors made of Fe and sometimes Ni to transform thousands of molecules of substrate per second in a very selective and effective manner. Various methods have been proposed to wire these enzymes and related synthetic catalysts to nanoparticles or to electrodes;[1−13] some of these strategies rely on the entrapment of the catalyst onto or into a polymer film.[14−17]

A major problem with the use of metalloenzymes is that they are fragile and oxygen sensitive. A large body of work describes the reaction of hydrogenases with O_2 (see, e.g., refs 18−20), the identification[21−23] and characterization[3,24−28] of relatively resistant enzymes, and the use of protein engineering to increase the resistance of otherwise fragile enzymes.[29,30] Molecular catalysts and synthetic models of the active site of hydrogenase also decay under aerobic conditions.[31−34] Some of us have recently proposed an entirely new strategy for getting around the problem of O_2-sensitivity, which should eventually prove applicable with various enzymes and synthetic catalysts. Resistance to O_2 is afforded by a redox hydrogel film that entraps the enzyme and prevents the deactivating molecules from reaching the active catalyst.[35] The protection of hydrogenases against O_2 was demonstrated, but much still needs to be understood before one becomes able to improve the design of these hydrogel films in a rational manner.

Understanding how the hydrogel protects the enzyme against O_2 requires that the evolution of the distribution of the different species in the film be calculated. This is challenging because the concentration profiles are the solution of a set of at least four coupled, nonlinear differential equations that describe the diffusion and reaction of the redox mediator, the different forms of the enzyme, the substrate and the inhibitor. Here we tackle the challenge of calculating the concentration profiles and analyzing the effect of exposing the film to O_2, and we quantitatively compare the experimental results with the model. We explain why a transient exposure to O_2 has a small, time-independent and fully *reversible* effect on the catalytic H_2-oxidation current, even if the inactivation of the enzyme by O_2 is *irreversible*. Our analysis is useful for determining which parameters have to be optimized to further improve the

Received: February 9, 2015
Published: April 2, 2015

DOI: 10.1021/jacs.5b01194
J. Am. Chem. Soc. 2015, 137, 5494−5505

properties of the enzyme/hydrogel electrode, as we anticipate the use of such films with O_2-sensitive catalysts other than hydrogenases.

2. EXPERIMENTAL METHODS

Polymer Synthesis. Water was removed from the commercial polyethylenimine polymer backbone (P3143 from Sigma-Aldrich, 50 wt %/vol in H_2O, M_n = 60 000, M_w = 750 000) under high vacuum at room temperature. Afterward, the dry polyethylenimine polymer (10 mg) was dissolved in dry dimethyl sulfoxide (DMSO) (4.3 mL) under sonication. The viologen monomer (1-(3-(acetylthio)propyl)-1′-(3-isothiocyanatopropyl)-[4,4′-bipyridine]-1,1′-diium iodide bromide,[35] 89 mg, 0.153 mmol) was then added to the polymer solution, and the mixture was stirred at room temperature for 24 h under argon atmosphere. DMSO was then removed by the application of high vacuum at room temperature. The resulting redox polymer was dissolved in water and filtered (molecular weight cutoff 5 kDa). Filtration was performed until the viologen monomers could not be detected in the filtrate upon the addition of sodium dithionite (sodium dithionite reduces the viologen to the radical cation which induces a blue color). The filtered polymer was concentrated to 15 mg/mL and used without further purification. The viologen monomer (M_w = 580.3 g/mol) coupled to the backbone represent 61 ± 4% (n = 3) of the total polymer mass based on UV−vis quantification. ^{1}H NMR (200 MHz, D_2O) δ 9.21 (m), 8.62 (m), 4.94 (m), 3.86 (m), 3.65 (m), 3.00 (t, 18), 2.74 (s), 2.60−2.32 (m), 2.40 (s).

Hydrogenase−Viologen Polymer Film Formation on Glassy Carbon Electrode Surface. The [NiFe]-hydrogenase from *Desulvofibrio vulgaris* MF[36] was purified as described previously.[37,38]

The hydrogenase was immobilized via physical entrapment in the polymer network. For this, an aqueous suspension of the viologen modified polymer (13.3 μL, 15 mg/mL) and the enzyme (3 μL, 200 μM in 10 mM MES buffer, pH 6.8) were mixed and applied to the glassy carbon electrode surface (4 mm diameter). The polymer cross-linking via disulfide bond formation was accelerated by adding Tris buffer to the solution droplet on the electrode surface (1 μL, pH 9, 100 mM). The electrode was stored at 4 °C in a closed vessel overnight to allow for hydrogel formation within the droplet. After 12 h the solution became turbid due to gel formation and was then left to dry in air at room temperature. The amount of polymer and enzyme used in this particular case yield a film thickness of 188 μm (based on the linear relation between the two shown in Supporting Information, Figure S5). Further films with various thickness were prepared by adjusting the amount of polymer and hydrogenase. In all cases the polymer to enzyme ratio was kept constant.

To evaluate the amount of enzyme in the film, we subtracted the amount of enzyme that was *not* retained. The electrode prepared as described above was rotated at 2000 rpm in 2 mL of phosphate buffer (100 mM, pH 7) for 30 min. This "waste" was then concentrated using viva spin filters (10 K) to reach a volume of 55 μL. The protein concentration was determined using a Lowry assay, using commercial kits from BioRad (*DC* Assay) and from Pierce (BCA Assay).

Electrochemistry. All electrochemical measurements were carried out with a rotating-disc electrode setup. Gas mixtures of H_2, Ar, and O_2 were adjusted with mass-flow controllers. A Pt wire was used as counter electrode. A rotating glassy carbon electrode modified with the polymer-hydrogenase film was used as a working electrode. Before modification the glassy carbon surface was polished with 1, 0.3, and 0.05 μm alumina suspension followed by 5 min of sonication. All electrochemical measurements were performed in phosphate buffer (0.1 M, pH 7.0) at room temperature. The reference electrode was Ag/AgCl/3 M KCl. Potentials are converted to standard hydrogen electrode (SHE) using the correction $E_{SHE} = E_{Ag/AgCl/3\ M\ KCl} + 210$ mV.

Determination of the Apparent Electron Diffusion Coefficient (D_A). The interdigitated array (IDA) electrodes consist of N Au fingers equally shared in two arrays with a gap d between the fingers and center-to-center width p of a two finger segment. Two sets of IDA with different geometries were used. For the first set N = 30, d = 10 μm, and p = 20 μm, for the second set, N = 130, d = 3 μm, and p = 6 μm. A pseudoreference electrode made of Ag/AgCl (0.41 V vs SHE) was integrated in the IDA. The Au IDA electrodes were cleaned by cycling in H_2SO_4 (0.5 M) five times from −0.4 to 1.4 V vs the AgCl pseudoreference electrode at 100 mV/s. The electrodes were modified by drop-casting a solution of the viologen-modified polymer (0.5 μL, 0.75 mg/mL) in water. After drying, Tris buffer (0.5 μL, 100 mM, pH 9.0) was added, and the electrode was left to dry for 1 h in air at room temperature. The generator−collector measurements were performed with a bipotentiostat (Autolab PGSTAT302N with a BA module) in phosphate buffer (100 mM, pH 7.2) and KNO_3 (0.5 M) under argon. Glucose oxidase (1 mg/mL), catalase (1 mg/mL), and glucose (9 mg/mL) were added to remove oxygen traces from the solution.[39,40] The potential of the generator electrode was cycled between −0.4 and −0.85 V vs AgCl pseudo reference electrode at 0.1 mV/s, while the collector electrode was poised at −0.2 V.

Determination of Film Thickness (l). The hydrogel film consisting of the viologen polymer and hydrogenase was first fully reduced by applying a potential of −0.625 V vs Ag/AgCl in phosphate buffer (100 mM, pH 7.0) first under H_2 atmosphere (100%) for 30 min and then under Ar atmosphere for 15 min at 2000 rpm. The rotation was then stopped and the potential was stepped to 0 V vs Ag/AgCl for several hours depending on film thickness. The film thickness was determined from the charge obtained for the complete oxidation of the initially fully reduced film, and from the concentration of viologen in the film.

Simulations. The system of four differential equations was solved analytically (see hereafter and Supporting Information, eq S5) or numerically using an in-house program that uses an implicit finite difference method, fourth order in time and first order in space, on a uniform grid ($\delta\xi = 10^{-4}$). The numerical data sets were handled with other in-house programs called SOAS[41] and QSoas, available at www.qsoas.org.

3. RESULTS

The Model. We built upon the model of an enzyme in a thin film described by Bartlett,[42] where the enzyme E is assumed to be immobilized, and its concentration is uniform through the thickness l of the film. The reactions of the enzyme are depicted in Figure 1. The substrate S is free to diffuse through the film, with a diffusion coefficient D_S. The mediator is immobilized within the film, reversibly oxidized at the electrode/polymer interface (eq 1a), and electron hopping

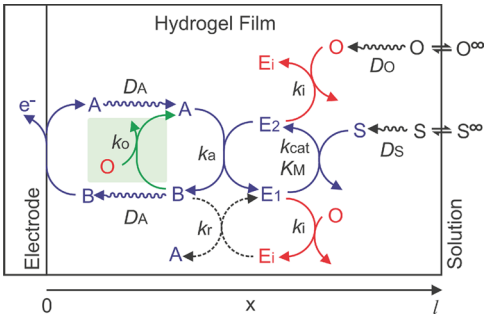

Figure 1. Schematic of an enzyme-electrode showing the processes considered in the model: in red the inactivation reaction, and in green the protection process. Diffusion of mediator (A and B), substrate hydrogen (S) and oxygen (O) occur within the film with diffusion coefficients D_A, D_S, and D_O, respectively. The homogeneous kinetics (eqs 1b−1g) occurs throughout the film from x = 0 (electrode surface) to x = l (film/solution interface). The reduced mediator (B) is reoxidized to produce A at the electrode surface (eq 1a). E_1, E_2, and E_i are the oxidized, reduced, and inactive forms of the enzyme, respectively. The same system but without the O_2-dependent reactions (blue arrows here, eqs 1a−1c only) was considered by Bartlett et al. in ref 42.

DOI: 10.1021/jacs.5b01194
J. Am. Chem. Soc. 2015, 137, 5494−5505

between adjacent redox sites behaves like a diffusional transport (section 4.3.4 in ref 43) with a diffusion coefficient D_A. The reduced enzyme (E_2) reacts with the oxidized mediator (A), and the oxidized enzyme (E_1) reacts with substrate S according to Michaelis–Menten kinetics (eqs 1b and 1c). Bartlett et al. have thoroughly investigated the steady-state solutions of this system, using both analytical[42] and numerical methods.[44] The kinetic case diagram in ref 42 (reproduced with permission as Supporting Information, Figure S1), predicts which concentration profiles are observed for given values of the parameters of the system.

The system bears much resemblance with the models previously examined by Andrieux and Savéant and co-workers where the catalyst is also the immobilized species that transfers electrons (ref 45 and refs therein). A recent development concerns the prediction of Tafel plots in the case of proton-coupled electron hopping through the film as rate controlling factors, and no limitation by substrate diffusion.[12]

To account for the experiments described in the recent *Nature Chemistry* paper (ref 35), we needed to add to Bartlett's model the reactions that describe the effects of O_2: the inactivation of the enzyme by O_2 (O), to form an inactive form of the enzyme E_i (eqs 1d and 1e, red arrows in Figure 1), its reactivation upon reaction with reduced mediator B (eq 1g, dashed arrow in Figure 1), and the oxidation of the viologen by O_2 (eq 1f, green arrow in Figure 1). Dioxygen diffuses through the film with a diffusion coefficient D_O.

The complete kinetic scheme therefore reads

$$\mathrm{B} \xrightarrow{\text{fast}} \mathrm{A} + e^- \quad (1a)$$

$$\mathrm{E_2} + \mathrm{A} \xrightarrow{k_a} \mathrm{E_1} + \mathrm{B} \quad (1b)$$

$$\mathrm{E_1} + \mathrm{S} \xrightarrow{k_{cat}/(K_m+S)} \mathrm{E_2} \quad (1c)$$

$$\mathrm{E_1} + \mathrm{O} \xrightarrow{k_i} \mathrm{E}_i \quad (1d)$$

$$\mathrm{E_2} + \mathrm{O} \xrightarrow{k_i} \mathrm{E}_i \quad (1e)$$

$$\mathrm{B} + \mathrm{O} \xrightarrow{k_o} \mathrm{A} \quad (1f)$$

$$\mathrm{E}_i + \mathrm{B} \xrightarrow{k_r} \mathrm{E_1} + \mathrm{A} \quad (1g)$$

All reactions but the first are bimolecular (k_a, $k_{cat}/(K_m+S)$, k_i, k_o, k_r are second-order rate constants). We treat the system assuming an infinite planar electrode (1D, linear geometry) and we note x the distance from the electrode surface, l the film thickness. The corresponding set of differential equations is given in section S1. The boundary conditions are as follows: fixed concentrations of S and O_2 at $x = l$; zero flux of A and B at $x = l$; zero flux of S and O_2 at $x = 0$ and, assuming that the electrode potential is high enough, $B = 0$ at $x = 0$. We assume that the concentrations of substrate and inhibitor in the solution outside of the film are homogeneous, an assumption which is valid for high electrode rotation rates, and that partition coefficients (solution to film) are equal to 1 for both hydrogen and oxygen.

In the model described above, the following items were not included: the reversibility of eqs 1b, 1c and 1g, the redox stoichiometry (two-electron) of the reaction of the enzyme with H_2, and the details about the kinetics of formation of the inactive states (the anaerobic or aerobic oxidation of [NiFe]-hydrogenases actually produces more than one inactive state, which reactivate under reductive conditions at different rates, cf. ref 18 and refs therein). The final form of the mathematical model was composed of 5 coupled differential equations, which included 16 independent parameters (three diffusion coefficient, 4 concentrations, 7 kinetic parameters, film thickness, and time; not counting the electrode potential).

To analyze the behavior of the reaction–diffusion system, we chose the following set of dimensionless variables: $a = A/A^\Sigma$, $b = B/A^\Sigma$, $e = E/A^\Sigma$, $o = O/A^\Sigma$, $s = S/A^\Sigma$, so that all concentrations are normalized with respect to the total concentration of mediator A^Σ; $\xi = x/l$ is the distance from the electrode/film interface normalized by the thickness of the film; the time $\tau = t \times k_a E^\Sigma$ is normalized by the time scale of the oxidative catalytic half cycle (eq 1b). This leads to defining the dimensionless parameters in Table 1, where superscript ∞ denotes the concentration in the bulk solution. The dimensionless set of differential equations is given in section S2 of the Supporting Information. Since inhibition by O_2 is much slower than turnover, it is useful to introduce the dimensionless concentration of active enzyme ($e_a = e_1 + e_2$, $e_a + e_i = \epsilon$) and to make the steady-state assumption on e_1 and e_2, as described in Supporting Information section S3.

Table 1. Definition and Values of the Dimensionless Parameters of the Model Used in Simulation 1 (∗), Figure 5, and Simulation 2 (∗∗), Figure 6

parameter	definition	value
κ	$l(k_a E^\Sigma/D_A)^{1/2}$	10^3
μ	A^Σ/K_m	150
κ_i	$k_i A^\Sigma/(k_a E^\Sigma)$	60
κ_o	$k_o A^\Sigma/(k_a E^\Sigma)$	1500
κ_r	$k_r A^\Sigma/(k_a E^\Sigma)$	0
ϵ	E^Σ/A^Σ	2.5×10^{-3}
δ^S	D_S/D_A	10^4
δ^O	D_O/D_A	4×10^3
α	$k_a K_m/k_{cat}$	10^{-3}
o^∞	O^∞/A^Σ	8×10^{-6}∗ or 8×10^{-4}∗∗
s^∞	S^∞/A^Σ	0.015

Finally, the system reduces to a set of only four differential equations (Supporting Information eq S5) that describe the irreversible, bimolecular reactions of four independent species (e_a, a, o, and s, taking into account that $e_i = \epsilon - e_a$ and $b = 1 - a$).

$$\mathrm{e}_a + o \xrightarrow{\kappa_i} e_i \quad (2a)$$

$$e_i + b \xrightarrow{\kappa_r} \mathrm{e}_a + a \quad (2b)$$

$$b + o \xrightarrow{\kappa_o} a \quad (2c)$$

$$a + s \xrightarrow{\mathrm{e}_a/[\epsilon(a\alpha(1+\mu s)+s)]} b \quad (2d)$$

The species have the following dimensionless diffusion coefficients $D_{e_i} = D_{e_a} = 0$, $D_b = D_a = 1/\kappa^2$, $D_o = \delta^O/\kappa^2$, $D_s = \delta^S/\kappa^2$. For example, the O_2 concentration profile is the solution of

$$\frac{\mathrm{d}o}{\mathrm{d}\tau} = \frac{\delta^O}{\kappa^2}\frac{\mathrm{d}^2 o}{\mathrm{d}\xi^2} - \kappa_i o \mathrm{e}_a - \kappa_o o(1-a) \quad (3)$$

The dimensional current density J/F (counted as positive for an oxidation reaction) is related to the dimensionless current $j = \kappa^{-2}\mathrm{d}a/\mathrm{d}\xi|_{\xi=0}$ by the relation

DOI: 10.1021/jacs.5b01194
J. Am. Chem. Soc. 2015, 137, 5494–5505

$$J/F = j \times lk_a E^{\Sigma} A^{\Sigma} \quad (4)$$

To use the above model in the context of the experiments in ref 35, we had to evaluate all the nondimensional parameters. We do so hereafter, based on the experimental determination of the values of D_A, A^{Σ}, E^{Σ}, and l, and the use of literature values of the kinetic parameters.

Experimental Determination of the Electron Diffusion Coefficient (D_A). We used interdigitated electrode arrays (IDA) in a generator-collector mode to determine the value of D_A.[46] Thin films of the viologen-based polymer were deposited on the IDA. The films were prepared without hydrogenase to avoid interference from catalytic H_2 evolution. We used AFM to confirm that the films cover the IDA and the gaps between the electrodes completely (Supporting Information, Figure S2A,B). The thickness of the dry film is about 20 nm according to a line scan (Figure S2C) over an area in which the polymer film was previously removed with the AFM tip (Figure S2A). Hence the dimension of the film in the swollen state is anticipated to remain within the dimension range of the electrode thickness (150 nm) and well below the dimension of the gap (d = 10 μm) between two fingers. Under these conditions, D_A can be calculated from the charge (Q) for complete electrolysis of the redox couple and from the limiting current (i_L) at the collector electrode:[46]

$$D_A = \frac{i_L dp}{Q} \frac{N}{N-1} \quad (5)$$

where N is the number of fingers in the IDA and p is the center-to-center width of a two-finger segment. Slow potential cyclic voltammograms (CVs) of the two electrodes shortened together display nearly symmetrical anodic and cathodic current responses, with low peak separation (Figure 2A) and the peak currents are proportional to scan rate (Supporting Information, Figure S3), indicating complete electrolysis of the viologen film. The apparent shifts of the reduction potential of the viologen result from fluctuations in the potential of the pseudoreference electrode. Q was extracted from the area under the cathodic curve (one-electron conversion of A to B). Using the generator-collector mode, the generator electrode was swept toward negative potential to reduce A while the collector electrode was maintained at a potential positive enough to reoxidize B. The formation of crossed concentration gradients of the A/B couple resulted in a steady state current (i_L) at the collector electrode (Figure 2B). The value of D_A calculated from i_L and Q was independent of electrolyte concentration and independent of the gap width and geometry of the IDAs.

The average value of D_A, obtained by repeating the experiments with 4 different IDAs, was (4.7 ± 1.7) 10^{-9} cm^2 s^{-1}.

Determination of the Viologen Concentration in the Film (A^{Σ}). We obtained A^{Σ} in the swollen film from fast scan cyclic voltammograms that are characteristic of semi-infinite planar diffusion conditions (Supporting Information, Figure S4A). Figure S4B shows the plot of the voltammetric peak currents (i_p) against the square root of the scan rates ($\nu^{1/2}$), the slope of which gives the product A^{Σ} $(D_A)^{1/2}$ (ref 47), according to the Randles–Sevcik equation:

$$A^{\Sigma}\sqrt{D_A} = i_p/0.4463F\mathcal{A}\sqrt{F\nu/RT} \quad (6)$$

Here, F, R and T have their usual meaning, ν is the scan rate, and $\mathcal{A}$ is the electrode surface.[48]

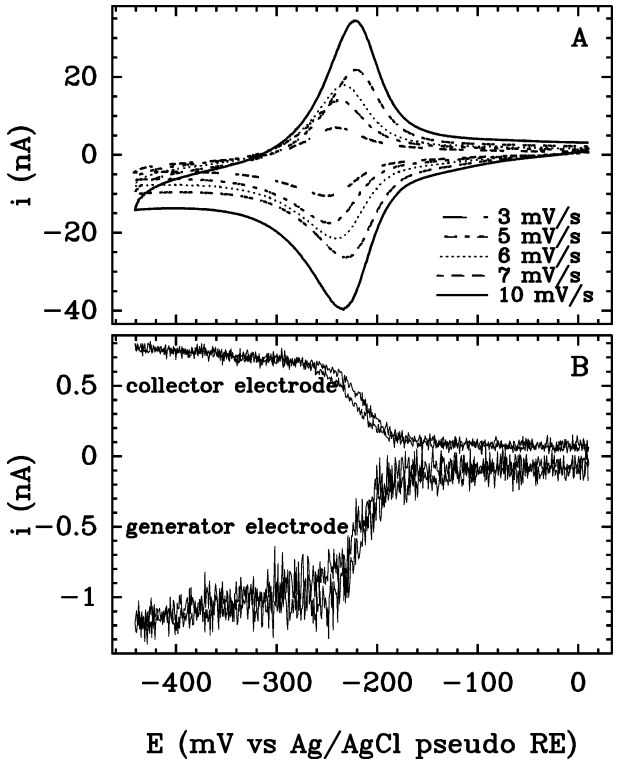

Figure 2. Interdigitated electrodes array (IDA) modified with viologen polymer film for determination of D_A. (A) Cyclic voltammograms at slow scan rates (from 3 mV/s to 10 mV/s) in the generator–generator mode. (B) Cyclic voltammogram (0.1 mV/s) at the generator electrode and current response at the collector electrode (applied potential −0.2 V vs Ag/AgCl pseudo-RE) in the generator–collector mode. The measurements were performed in phosphate buffer (100 mM, pH 7.2) and KNO_3 (0.5 M) under strictly anaerobic conditions.

We were able to determine the value A^{Σ} = 59 ± 11 mM, from the product A^{Σ} $(D_A)^{1/2}$ obtained from the cyclic voltammetry experiments with 10 different electrodes (l ranging between 35 and 375 μm) and using the value for D_A determined from the interdigitated electrodes array experiments.

Determination of the Film Thickness (l). The determination of film thickness for films in the dry state is well established.[49] However, direct measurement of the highly solvated and flexible hydrogels, though less straightforward, is preferable. In general the solvated film thickness is calculated from its thickness in the dry state and from its degree of swelling upon exposure to the solvent.[47] In these experiments, however, we were able to use a combination of electrochemical measurements to determine the thickness of film entirely in the solvated state, that is, under conditions that are fully relevant to the modeling of the electrocatalytic film. We proceeded as follows.

The film thickness l can be expressed as

$$l = V/\mathcal{A} = Q/(A^{\Sigma}\mathcal{A}F) \quad (7)$$

where V is the volume of the film, $\mathcal{A}$ is the electrode surface, Q is the charge passed upon complete electrolysis of the film, and A^{Σ} is the concentration of viologen in the film as determined by cyclic voltammetry. We determined Q by prolonged potential step chronoamperometry (Supporting Information, Figure S5A,B) for the complete oxidation of an initially fully reduced film ($B = A^{\Sigma}$, $A = 0$). The measurements were performed with

DOI: 10.1021/jacs.5b01194
J. Am. Chem. Soc. 2015, 137, 5494–5505

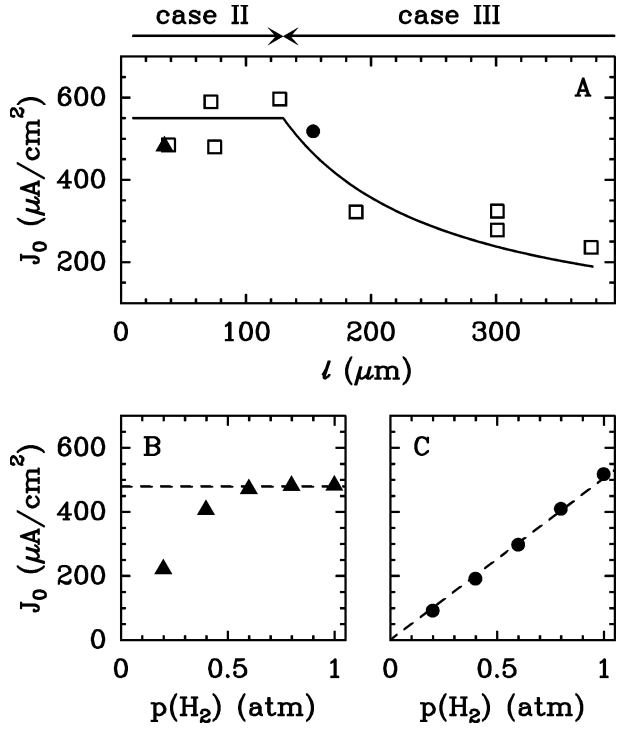

Figure 3. Dependence of the anaerobic, steady-state, catalytic H_2-oxidation current on film thickness, at one atm of H_2 (panel A) and against H_2 pressure, for l = 35 μm (panel B) and l = 154 μm (panel C). The filled symbols in Panel A indicate which films were used for the experiments in panels B and C. The model in panel A is eq 8 for l < 130 μm and eq 9 for l > 130 μm. The dashed lines in panels B and C are consistent with eqs 8 and 9, respectively. Parameters: T = 22 °C, pH = 7, bulk concentration of H_2 = 1 mM, electrode potential, 210 mV vs SHE, electrode rotation rate, 2000 rpm.

three electrodes modified with different amounts of polymer. We observed that the calculated film thicknesses (between 35 and 127 μm) were proportional to the amount of polymer deposited for the film formation (Figure S5C). This linear relation was used to determine the thickness of all other films.

Estimation of the Approximate Values of the Dimensionless Parameters of the Model. From the above-described experiments, we calculated A^{Σ} = 60 mM. Therefore, a saturating concentration of H_2 (S^{∞} = 1 mM) corresponds to $s^{\infty} = S^{\infty}/A^{\Sigma} = 0.015$, and 5% O_2 to $o^{\infty} = O^{\infty}/A^{\Sigma} = 8 \times 10^{-4}$. With a value of K_m for H_2 of about 10 μM (ref 50), we obtain $\mu = A^{\Sigma}/K_m = 150$.

An estimate of the value of E^{Σ} can be calculated by subtracting from the amount of enzyme that is used to make a film, the amount of enzyme that was not retained in the film, measured in the waste using a Lowry assay. With three different electrodes, we obtained an average of E^{Σ} = 0.15 ± 0.01 mM, hence $\epsilon = E^{\Sigma}/A^{\Sigma} = 2.5 \times 10^{-3}$.

Figure 3A shows the catalytic H_2-oxidation current plotted as a function of film thickness. The change from a plateau at low l, to a current that decreases as l increases, is characteristic of the transition from case II to case III according to Bartlett's work (Supporting Information, Figure S1). In case II, the concentration of substrate H_2 is homogeneous in the film, and the concentration of oxidized mediator decreases exponentially as a function of the distance to the electrode (x). The catalytic current is independent of H_2 concentration in the bulk (Table 3 in ref 42):

$$J_0^{II}/F = \sqrt{D_A}A^{\Sigma}\sqrt{k_a E^{\Sigma}} \quad (8)$$

For larger values of l, the system behaves as in case III, where the current is proportional to the reciprocal of l (Table 3 in ref 42):

$$J_0^{III}/F = \frac{D_A A^{\Sigma} + D_S S^{\infty}}{l} \quad (9)$$

The value J_0 = 550 μA cm^{-2} for l =130 μm (Figure 3A) is much greater than $FD_A A^{\Sigma}/l$, which means that $D_A A^{\Sigma} \ll D_S S^{\infty}$, hence:

$$J_0^{III}/F \approx D_S S^{\infty}/l \quad (10)$$

Panels B and C of Figure 3 show the dependence of the current on bulk H_2 concentration for two films, l = 35 μm in panel B and l =154 μm in panel C. If l is large enough that the current at one atm of H_2 is proportional to the reciprocal of l, then the current is proportional to the bulk concentration of H_2 (panel C), as predicted by eq 10. If l is small enough that the current at one atm of H_2 is independent of l, then the current is also independent of H_2 pressure at high H_2 pressure, but it decreases at low H_2 pressure when substrate transport in the film becomes limiting (panel B). All this is consistent with the conclusion in ref 42 that the transition from case II to III occurs when $\kappa/(1 + \delta^S s^{\infty})$ becomes greater than 1 (Supporting Information, Figure S1), meaning that decreasing the substrate concentration in the bulk pushes the system into case III.

Hereafter, we focus on thick films, that behave as in case III, and the current is given by eq 10. The value J_0 = 550 μA cm^{-2} for l = 130 μm, 1 atm of H_2 (Figure 3A), gives $D_S S^{\infty} = 7 \times 10^{-11}$ mol cm^{-1} s^{-1}, which is very close to what we expect from the values of S^{∞} and D_S in solution: $S^{\infty} = 10^{-6}$ mol/cm^3 and $D_S = 5 \times 10^{-5}$ cm^2/s (refs 51 and 52). Using $D_S = 5 \times 10^{-5}$ cm^2 s^{-1} and $D_A = 5 \times 10^{-9}$ cm^2 s^{-1}, we obtain $\delta^S = 10^4$, and assuming that O_2 diffuses in the film as fast as in solution, $D_O = 2.4 \times 10^{-5}$ cm^2 s^{-1} (ref 53), δ^O = 5000.

Using the conclusion that the transition between cases II and III occurs at $\kappa = 1 + \delta^S s^{\infty}$ (Table 2 in ref 42), we deduce that for films in case III, κ must be much greater than $1 + \delta^S s^{\infty} = 151$. We shall assume $\kappa = 10^3$.

Since k_a equates the ratio of k_{cat} over the Michaelis constant relative to the mediator, we deduce $\alpha = K_m^{H_2}/K_m^A$, and using the value of K_m^A determined in ref 54 we estimate $\alpha = 10^{-3}$.

To include in the model the kinetics of reaction with O_2, considering the definition of the dimensionless parameters listed in Table 1, we need to determine the value of $k_a E^{\Sigma}$. We do this from the value of the H_2-oxidation plateau current in Figure 3 and eq 8, because this estimate of $k_a E^{\Sigma}$ only relies on the value of $(D_A)^{1/2}A^{\Sigma}$ which is deduced from the voltammetry in a very straightforward manner (eq 6). With J^{II}_0 = 550 μA/cm^{-2}, we obtain $k_a E^{\Sigma}$ = 40 s^{-1}. Using the value of k_i = 40 s^{-1} mM$(O_2)^{-1}$ (ref 50), we deduce $\kappa_i = k_i A^{\Sigma}/k_a E^{\Sigma} \approx 60$. In ref 55 De Lacey and co-workers measured a first-order reactivation rate constant of about 2×10^{-4} s^{-1} for the so-called Ni−SU inactive state of [NiFe]-hydrogenase, in the presence of 1 mM methyl viologen and benzyl viologen. Assuming that the activation rate constant is proportional to the total concentration of viologen, we calculate $\kappa_r = k_a A^{\Sigma}/k_a E^{\Sigma} \approx 3 \times 10^{-4}$. This reaction is so slow that we chose to neglect it by setting κ_r = 0. Last, using the value $k_o = 10^3$ s^{-1} mM^{-1} in ref 56 for the reduction of O_2 to H_2O_2, we obtain $\kappa_o \approx 1500$. The dimensionless duration of the exposure to O_2, δt = 300 s in the experiments of Figure 9A, is $\delta\tau = \delta t \times k_a E^{\Sigma} = 12 \times 10^3$.

DOI: 10.1021/jacs.5b01194
J. Am. Chem. Soc. 2015, 137, 5494−5505

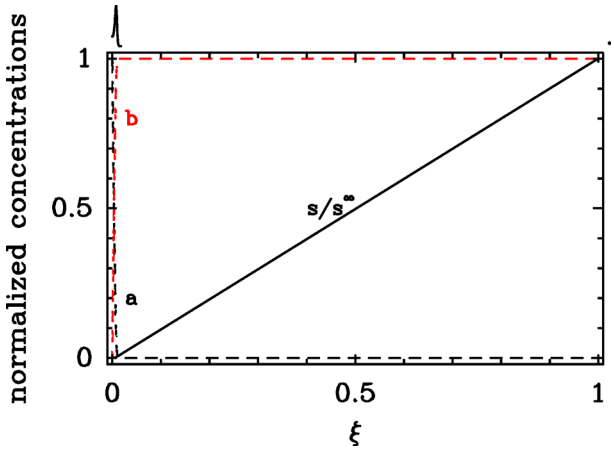

Figure 4. Steady-state, anaerobic concentration profiles in the hydrogenase/redox-polymer film, plotted as a function of the normalized distance to the electrode (the electrode surface is at $\xi = 0$, the interface between the film and the solution is at $\xi = 1$). $a = 1 - b$ is the normalized concentration of oxidized mediator, s/s^{∞} is the normalized concentration of substrate H_2. On top of the plot, the black line shows the rate of catalysis (the last term in Supporting Information, eq S5c). The profiles were obtained by simulating equation 2 for a set of parameters that is consistent with the experiments in ref 35 as indicated in Table 1, except $o^{\infty} = 0$.

The values of the parameters of the model are summarized in Table 1. Note that only the order of magnitude of these parameters is of interest here.

The Steady-State Current and Concentration Profiles in the Absence of O_2. Figure 4 shows the anaerobic, steady-state concentration profiles in the film, calculated for the set of parameters in Table 1 except that $o^{\infty} = 0$. As expected, the current is limited by the transport of H_2 and electrons in the film (case III in Supporting Information, Figure S1).

The reaction zone is very close to the electrode because $D_A A^{\Sigma} \ll D_S S^{\infty}$. Its position, ξ_r, defined as the value of ξ where a and $s\delta^S$ intersect, is obtained by equating the fluxes of b and s at $\xi = \xi_r$. From $\delta^S s^{\infty}/(1 - \xi_r) = 1/\xi_r$, we obtain

$$j_0 = (1 + \delta^S s^{\infty})/\kappa^2 \tag{11}$$

which is the dimensionless version of eq 9. The steady-state H_2 oxidation current is proportional to the bulk concentration of H_2, proportional to the reciprocal of film thickness, and independent of enzyme concentration.

The Progression of the Front of Inactive Enzyme When the Film Is Exposed to O_2. Starting from the steady-state concentration profiles in Figure 4, we simulated the effect of exposing the film to O_2, examining two different cases: one that is very simple, where the bulk concentration of oxygen is much lower than in our experiments ($o^{\infty} = 5 \times 10^{-6}$), and another case that is realistic ($o^{\infty} = 5 \times 10^{-4}$). Figures 5 and 6 show the corresponding snapshots of the concentration profiles (including O_2, shown as a dotted line) at time $\tau = 10^{10}$ after the beginning of exposure to O_2. The complex effect of O_2 is clear: the inhibitor oxidizes the mediator (dashed line) and reacts with the active enzyme, which is converted into the inactive form (dot-dash line) in a thin layer near the film/solution interface.

We observe in the simulations of Figures 5 and 6 that the concentration profile of inactivated enzyme is very sharp (dot-dash line). We define ξ_f as the dimensionless position of the

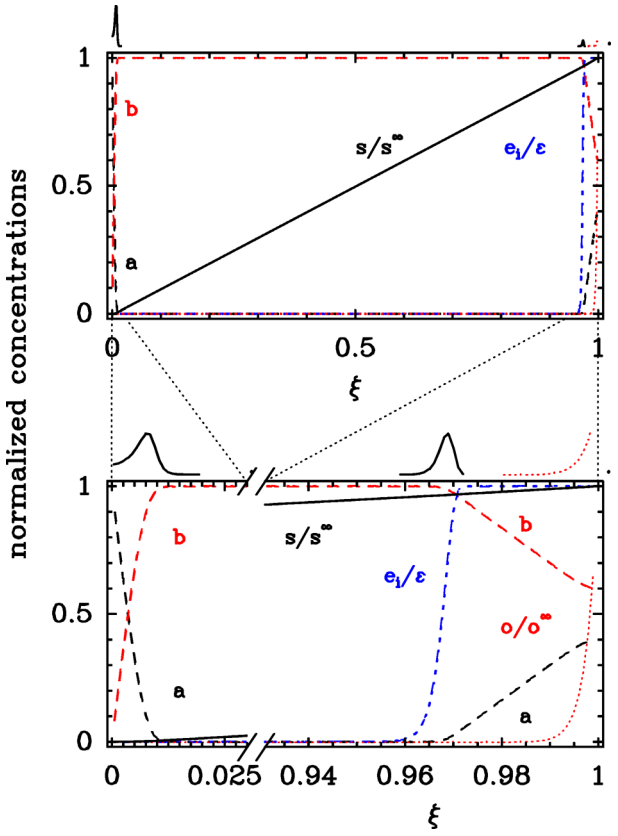

Figure 5. Concentration profiles in the hydrogenase/redox-polymer film exposed to a low concentration of O_2. The top panel shows the whole profiles, the bottom panels zoom on the regions of the film near the electrode/film and film/solution interface. a (black, dashed line) and $b = 1 - a$ (red, dashed line) are the concentrations of oxidized and reduced mediator, respectively; s/s^{∞} (plain line) and o/o^{∞} (red, dotted line) are the normalized concentrations of substrate H_2 and inhibitor O_2, respectively, e_i/ϵ (dash-dot line) is the concentration of inactive enzyme. On top of each plot, the black line shows the rate of catalysis (the last term in eq S5c) and the red, dotted line shows the rate of O_2 reduction (the last term in eqs 3 and S5d), on the same scale. The profiles where obtained by simulating eqs 2, for the set of parameters number 1, as indicated in Table 1. They are shown at time $\tau = 10^{10}$ after the film is exposed to O_2.

front of inactive enzyme ($\xi_f \approx 0.965$ in Figure 5B, $\xi_f \approx 0.81$ in Figure 6B). The enzyme is inactive on one side of this front ($\xi > \xi_f$), and active and reduced on the other side ($\xi < \xi_f$). Figure 7 shows that in both simulations, the position of the front of inactive enzyme, ξ_f, varies in proportion to the logarithm of time (that is, more and more slowly). This variation is unexpectedly simple, and we aimed at understanding why that is so and what determines the rate of progression of the front, $d\xi_f/d \log \tau$.

We start by examining the simple case observed with the first set of parameters, where the O_2 concentration is very low. In this hypothetical case, the reaction between O_2 and B at the interface does not significantly deplete the concentration of B near the film/solution interface (Figure 5B). Regarding the O_2 concentration profile (dotted line), a steady-state is established by mutual compensation of O_2 diffusion and reaction with the reduced mediator. The steady-state profile is the solution of

$$\frac{do}{d\tau} = \frac{\delta^O}{\kappa^2}\frac{d^2o}{d\xi^2} - \kappa_o o = 0 \tag{12}$$

DOI: 10.1021/jacs.5b01194
J. Am. Chem. Soc. 2015, 137, 5494−5505

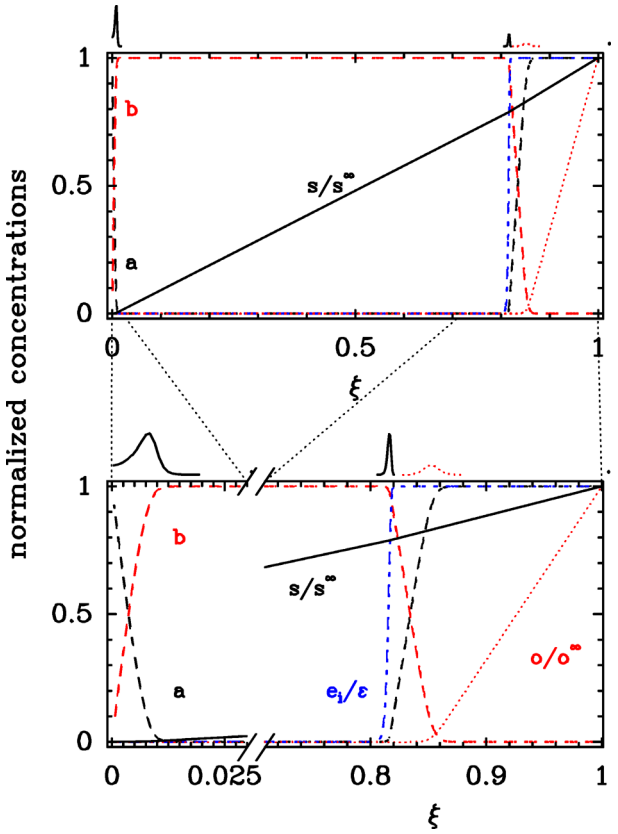

Figure 6. Concentration profiles and rates of catalysis and O_2 reduction in the hydrogenase/redox–polymer film exposed to a high concentration of O_2 (see also Figure 5). The profiles were obtained by solving eqs 2, for the set of parameters number 2, as indicated in Table 1. They are shown at time $\tau = 10^{10}$ after the film is exposed to O_2.

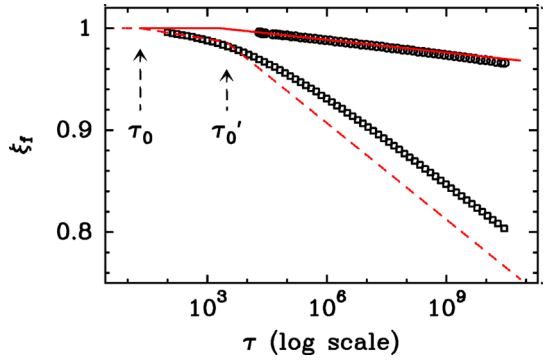

Figure 7. Numerical evidence that the progression of the front of inactive enzyme (after the film is exposed to O_2) is slow. The circles and squares show the change in time of the position of the front of inactive enzyme in simulations 1 and 2, respectively. The plain line is eq 15 and the dashed line is eq 20.

We have neglected the term $-\kappa_i o e_a$ in eq 3 because e_a is small, lower than ϵ; this approximation means that the reaction between the active enzyme and O_2 does not significantly contribute to the depletion of O_2 in the film. The solution of $d^2o/d\xi^2 \propto o$ (eq 12) is an exponential function and the O_2 profile is simply obtained by using the boundary conditions $o(\xi = 1) = o^\infty$:

$$o(\xi) = o^\infty \exp^{-(1-\xi)/\lambda_o} \tag{13a}$$

$$\lambda_o = \kappa^{-1}\sqrt{\delta^O/\kappa_o} \tag{13b}$$

where λ_o is a penetration length for O_2.

Since the concentration profile of inactive enzyme is essentially a step function at ξ_f, the total amount of enzyme inactivated per unit of time equates to the change in position of the front:

$$\frac{d\xi_f}{d\tau} = \int_{\xi=0}^{\xi=\xi_f} \kappa_i o(\xi)\, d\xi \tag{14a}$$

$$= -\kappa_i o^\infty \lambda_o \exp^{-(1-\xi_f)/\lambda_o} \tag{14b}$$

Equation 14b is readily integrated, using the initial condition $\xi_f = 1$ at $\tau = \tau_0$, to obtain the position of the front as a function of time:

$$\xi_f(\tau) = 1 - \lambda_o \ln \frac{\tau}{\tau_0} \tag{15}$$

The lag phase τ_0 corresponds to the time during which e_i builds-up at the film/solution interface, with a pseudo-first-order rate constant $\kappa_i o^\infty$, until e_i $(\xi = 1) = 1$ at

$$\tau_0 = 1/\kappa_i o^\infty \tag{16}$$

Equation 15 is plotted as a plain line in Figure 7, alongside the empty circles that show the position of the front measured in simulation 1. The model only slightly underestimates the rate of progression of ξ_f because it neglects the depletion of the reduced mediator in the aerobic reaction layer (Figure 5).

We now examine the realistic case where o^∞ is so large that the depletion of reduced mediator at the film/solution interface is significant, as indeed observed in the simulation of Figure 6. The schematic representation of Figure 8 shows ξ_r, the position of the catalytic front where H_2 is oxidized in the inner layer (electrons being transferred to the electrode), and ξ_f, the position of the front of inactive enzyme; we also define ξ_m, the position of the O_2-reduction front in the outer layer (strictly, the intersection between b and $\delta^O o$). The simulation Figure 6 shows that at $\xi = \xi_m$, the concentrations of b and o are small. The fact that the reduction of O_2 is limited by the transport of O_2 and electrons in the outer layer imposes that

$$1 - \xi_m = (1 - \xi_f)\frac{\delta^O o^\infty}{1 + \delta^O o^\infty} \tag{17}$$

The rate of progression of ξ_f depends on the concentration of O_2 at ξ_f, which has to be evaluated. This is not as simple as in the previous case (eq 13a) because the O_2 concentration profile is not steady, and it is not a mere exponential function. It is a linear function (the solution of $d^2o/d\xi^2 = 0$) in the outer region where $b \approx 0$ ($0.85 < \xi < 1$ in the example of Figure 6), an Airy function[57] (the solution of $d^2o/d\xi^2 \propto o\xi$) in the region where b is a linear function of ξ ($0.8 < \xi < 0.85$ in Figure 6), and an exponential function (the solution of $d^2o/d\xi^2 \propto o$) in the inner part of the film where $b \approx 1$ ($\xi < 0.8$ in Figure 6). The calculations of the O_2 concentration profile and of the position of the front required considerable effort, as detailed in section S4. And yet the result of the calculation is rather simple:

$$d\xi_f/d\tau \propto \exp^{-(1-\xi_f)/\lambda_o'} \tag{18a}$$

$$\lambda_o' = \frac{3(1 + \delta^O o^\infty)}{2\kappa}\sqrt{\frac{\delta^O}{\kappa_o}} \tag{18b}$$

DOI: 10.1021/jacs.5b01194
J. Am. Chem. Soc. 2015, 137, 5494−5505

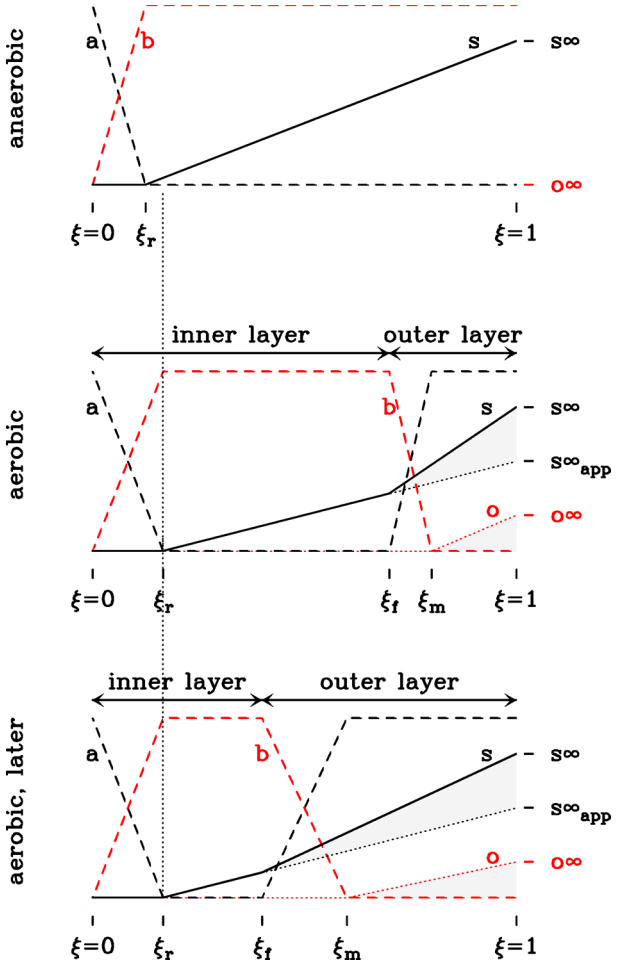

Figure 8. Schematic representation of the concentration profiles in the hydrogenase/polymer film, either under anaerobic conditions (top) or exposed to a large concentration of O_2 (middle and bottom). *a* is the oxidized mediator, *b* the reduced mediator, *s* the concentration of H_2, *o* the concentration of O_2. The vertical dotted line shows the variation of ξ_r that translates into a decrease in current. The gray triangles in the lower panels of Figure 8 represent the flux of H_2 that is lost in the short-circuit, the electrons being used to reduce the incoming O_2. The enzyme is irreversibly inactivated in the outer layer.

Integration gives

$$\xi_f(\tau) = 1 - \lambda_o' \ln \frac{\tau}{\tau_0'} \tag{19}$$

where τ_0' is the time it takes for b to be completely depleted in the outer layer, or, equivalently, for $1 - \xi_f$ to become greater than λ_o'. On shorter times, for $\tau_0 < \tau < \tau_0'$, we show in Supporting Information section S4.2 that everything happens as in the simpler case above, except that the depletion of b increases the O_2 penetration length by a factor $^3/_2$. We obtain the following expression for ξ_f:

$$1 - \xi_f(\tau) = 1 - \frac{3}{2}\lambda_o \ln \frac{\tau}{\tau_0} \quad \tau_0 < \tau < \tau_0' \tag{20a}$$

$$1 - \xi_f(\tau) = \lambda_o'\left(1 - \ln \frac{\tau}{\tau_0'}\right) \quad \tau > \tau_0' \tag{20b}$$

with τ_0 given by eq 16, and

$$\tau_0' = \tau_0 \exp(1 + \delta^O o^\infty) \tag{21}$$

Equation 20 is plotted as a dashed line in Figure 7, where the squares show the values of ξ_f in simulation 2. The very good agreement between the simulation and the prediction of eq 20 suggests that the above approximations and calculations are correct.

We conclude that, in this second case too, $1 - \xi_f$ increases in proportion to $\ln \tau$ according to

$$1 - \xi_f \propto \frac{3}{2}(1 + \delta^O o^\infty)\lambda_o \ln \tau \tag{22}$$

The Change in Current upon Exposure to O_2. Considering the case where the concentration of O_2 is low (simulation 1), the value of the current observed in the presence of O_2 can be calculated rather easily, by equating the fluxes of *a* at $\xi > \xi_f$ and *s* at $\xi > \xi_r$ (eq 23a), and the flux of *s* at $\xi < \xi_f$ and at $\xi > \xi_f$ (eq 23b). We note s_f the value of *s* at $\xi = \xi_f$.

$$j = \frac{1}{\kappa^2}\frac{1}{\xi_r} = \frac{\delta^S}{\kappa^2}\frac{s_f}{\xi_f - \xi_r} \tag{23a}$$

$$= \frac{\delta^S}{\kappa^2}\frac{s^\infty - s_f}{1 - \xi_f} - \frac{\delta^O o^\infty}{\kappa^2 \lambda_o} \tag{23b}$$

The values of s_f can be deduced as a function of ξ_f, to obtain

$$j(\tau) = \frac{1 + \delta^S s^\infty}{\kappa^2} - \frac{\delta^O o^\infty (1 - \xi_f(\tau))}{\lambda_o \kappa^2} \tag{24}$$

where $\xi_f(\tau)$ is given by eq 15 and τ_0 is given by eq 16.

If the concentration of O_2 is high, the expression for the incoming flux of O_2 is different because the outer O_2 profile is a line from $\xi = 1$ to $\xi = 1 - \xi_m$ (Figure 8), rather than an exponential function with a penetration length λ_o. Equation 23b is replaced with

$$\frac{1}{\kappa^2}\frac{1}{\xi_r} = \frac{\delta^S}{\kappa^2}\frac{s^\infty - s_f}{1 - \xi_f} - \frac{\delta^O o^\infty}{\kappa^2(1 - \xi_m)} \tag{25}$$

Combining eqs 17 and 25 gives the expression of the current, which is very simple and independent of τ, as indeed observed in experiments and simulations (Figure 9):

$$j = \frac{1 + \delta^S s^\infty}{\kappa^2} - \frac{1 + \delta^O o^\infty}{\kappa^2} \tag{26a}$$

$$\frac{j}{j_0} = \frac{\delta^S s^\infty - \delta^O o^\infty}{1 + \delta^S s^\infty} \tag{26b}$$

where j_0 is the dimensionless current in the absence of O_2, defined in eqs 9 and 11.

Figure 9 shows the change in current that results from exposing the film to 5% O_2. Panel A is an experimental result with repeated 300 s exposure to O_2 and panel B is a simulation with the set of parameters in Table 1, and an exposition to $o^\infty = 8 \times 10^{-4}$ for a time $\delta\tau = 12000$. The fact that the current reaches a steady-state value upon exposure to O_2 and completely recovers its initial value when O_2 is flushed out is clear both in the experiment and simulation.

In both panels in Figure 9, the dashed line shows the level of inhibition expected from eq 26b. That the agreement with the simulation is very good supports the derivation of eq 26b. The inhibition is slightly more pronounced in the experiment than the model predicts. The small discrepancy could have a number of causes, including D_O being overestimated, or D_S being

DOI: 10.1021/jacs.5b01194
J. Am. Chem. Soc. 2015, 137, 5494−5505

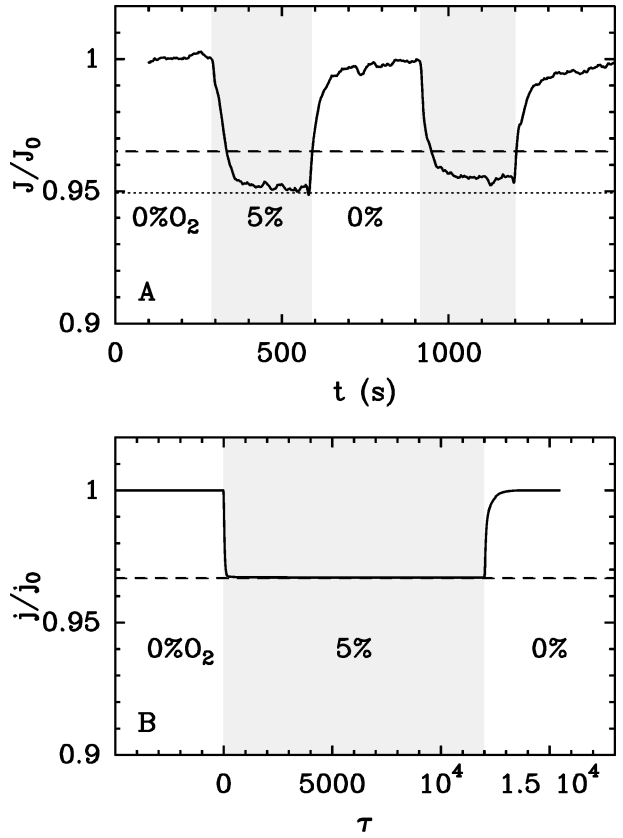

Figure 9. Change in H_2 oxidation current induced by exposure to 5% O_2, in experiments (panel A) and in a simulation (panel B). The dashed line in both panels marks the value of the current in the presence of O_2 calculated from eq 26 and the parameters whose values are estimated in the main text. The dotted line in panel A is the prediction of eq 26, assuming that $D_S S^\infty$ is 20% lower and $D_O O^\infty$ is 20% greater than our estimates. Experimental parameters for panel A: l = 275 μm, T = 22 °C, pH = 7, electrode rotation rate, 2000 rpm, electrode potential, 210 mV vs SHE. Parameters for the simulation in panel B: Those listed in Table 1, with $o^\infty = 8 \times 10^{-4}$.

underestimated, or the partitions of H_2 and O_2 being slightly different. Indeed, the dotted line in panel A shows the prediction of eq 9 assuming that $D_S S^\infty$ is 20% lower and $D_O O^\infty$ is 20% greater than our estimates.

4. DISCUSSION

We have examined, both theoretically and experimentally, the behavior of a planar hydrogel film containing a redox polymer and a redox enzyme, [NiFe]-hydrogenase, exposed to a solution containing the substrate of the enzyme (H_2) and an irreversible inhibitor which can be reduced by the redox polymer (O_2), as depicted in Figure 1.

To understand how the redox polymer protects the enzyme against inactivation by O_2,[35] we used a reaction-diffusion scheme that describes the evolution in time and space of the concentrations of mediator, substrate H_2, inhibitor O_2, and active enzyme (eq 1a). The same system *in the absence of inhibitor and under steady-state conditions* has already been fully described in the papers of Bartlett et al.[42] and Savéant et al.;[43,45] they have inventoried and discussed a variety of limiting cases, where either catalysis or transport of substrate and/or electrons limits the steady-state catalytic current (Supporting Information, Figure S1). The presence of O_2 makes the reaction-diffusion set of equations significantly more complex, because O_2 can react both with the enzyme and with the redox mediator. Moreover, in the cases we examined, the concentration profiles do not reach a steady state. (We expect that they would if the value of k_r in eq 1g was large enough, but we only considered k_r = 0.) We have shown that the evolution of the concentration profiles depends on the values of the 11 dimensionless parameters listed in Table 1. It was not our intention to examine all possible cases in this vast parameter space. Instead, we experimentaly determined the values of some parameters (the film thickness, l, the concentrations of viologen and enzyme in the film, A^Σ and E^Σ, and the diffusion coefficient of electrons, D_A), and we used literature values for the rate constants to determine the order of magnitude of each of the 11 parameters, and to focus on the case that corresponds to the experiments in ref 35 and Figure 9A. We chose to obtain the diffusion coefficient D_A from measurements carried out with interdigited electrodes in generator−collector mode (Figure 2);[46] the product $A^\Sigma(D_A)^{1/2}$ from noncatalytic voltammetry under semi-infinite planar diffusion conditions (Supporting Information, Figure S4); and the volume of the swollen film (hence, its thickness l) from the total charge measured in chronoamperometry experiments (Supporting Information, Figure S5). The D_A value of 4.7×10^{-9} cm^2 s^{-1} in the polymer film is in line with those observed for other types of redox hydrogel films.[46,47,58−60] The value of $A^\Sigma \approx 60$ mM was independent of film thickness, indicating uniform film properties for all modified electrodes. We calculated the values of l (ranging from 35 to 375 μm) from experiments carried out under the same conditions (buffer solution, applied potential) as those used to measure the catalytic H_2 oxidation current, to make sure the estimated parameters are as close as possible to those relevant for the catalytic experiments.

The exact value of the parameters in Table 1 is unimportant; it only matters that our estimates are of the right order of magnitude, so that the particular case that we consider is relevant. The calculated concentration profiles in Figure 4 show that the steady-state catalytic current obtained in the absence of O_2, the value of which is given by eq 9, is entirely limited by transport. This situation is that referred to as "case III" in ref 42 (Figure S1), or "S+E" in Savéant's work (e.g., Figure 4.19 in ref 43 or Figure 1 in ref 45); both mediator and substrate are consumed within the film, resulting in a change from mediator to substrate-limited kinetics through the film. We confirmed that the system behaves as predicted by our analysis by looking at the dependence of the steady-state H_2-oxidation current on bulk H_2-concentration and film thickness (Figure 3).

In the case that corresponds to the experiments in ref 35 and Figure 9A, there are three thin, parallel reaction planes in the film: one near the electrode, at ξ_r, where the oxidation of H_2 results in a catalytic current; one at ξ_f where a fraction of the incoming H_2 is oxidized to give electrons that are transferred to the third reaction front, at ξ_m, where the incoming O_2 is reduced. This is schematized in Figure 8.

That the portion of the film that is actually involved in catalysis is very small, and centered on a reaction front that is near the electrode/film interface (Figure 4 and eq 11), is the reason the effect of O_2 appears to be reversible in the experiments in Figure 9A, and in our model (Figure 9B) despite the assumption that the reaction of the enzyme with O_2 is irreversible (k_r = 0). Indeed, the enzyme molecules that are inactivated are those that are near the film/solution interface (x = l), but these enzyme molecules do not contribute to the

DOI: 10.1021/jacs.5b01194
J. Am. Chem. Soc. 2015, 137, 5494−5505

current under anaerobic conditions, and therefore, the current recovers its initial value when O_2 is flushed away from the cell solution.

Upon exposure to O_2, after a very short lag phase ($1/k_iO^\infty \approx 0.5$ s, eq 16), the thickness of the outer layer of inactive enzyme keeps increasing, but it does so very slowly, in proportion to the logarithm of time (Figure 7). This is fundamental, because the extremely slow progression of the inactive front affords long-term resistance to O_2. The reason the width of the inactive layer increases in proportion to $\log(t)$ is that the "tail" of the O_2 concentration profile is an exponential function. We could demonstrate that this is so in two different cases, (i) when the bulk concentration of O_2 is so low that the redox mediator is not significantly oxidized at the film/solution interface (Figure 5) and (ii) when the large bulk concentration of O_2 depletes the reduced mediator at the film/solution interface (Figure 6). In the former case, which corresponds to "pure kinetic conditions" for the reduction of O_2,[43] the steady-state O_2 concentration profile is a mere exponential decay with a penetration length $(D_O/k_oA^\Sigma)^{1/2}$ that reflects the competition between the diffusion and consumption of O_2 (eq 13). The latter case, exemplified in Figure 6 and schematized in Figure 8, corresponds to the experiments in ref 35. The O_2 profile is a linear function up to a certain depth (ξ_m), beyond which it decays *approximately* exponentially with a characteristic length given by eq 18b; solving the reaction−diffusion equations in that case is particularly demanding (Supporting Information, section S4). Figure 7 shows the very good agreement between the results of simulations and the predictions of the position of the front of inactive enzyme in the two situations.

The rate of progression of the front is surprisingly independent of the rate of aerobic inactivation (k_i in eqs 1d and 1e):

$$\frac{d(l - x_f)}{d \ln t} \approx \frac{3D_O^{3/2}O^\infty}{2k_o^{1/2}D_A A^{\Sigma^{3/2}}} \tag{27}$$

($x_f = \xi_f l$ is the position of the front of inactive enzyme). The inactivated layer thickens with a rate that depends on the bulk concentration and diffusion coefficient of O_2, and on the reciprocal of the concentration of mediator and electron diffusion coefficient.

The model predicts that despite the fact that the O_2 profile is not steady (ξ_f is a function of time, eq 20), the current *does* reach a steady-state value in the presence of O_2 (eq 26a), as indeed observed in experiments (Figure 9A). The reason for this is clear from Figure 8. The current is constant in the presence of O_2 because the gradient of s at $\xi = \xi_r$ is constant: it is as if there was no O_2 and the bulk concentration of s was constant and lower than s^∞ (s_{app}^∞ is this apparent bulk concentration of s). The gray triangles in the lower panels of Figure 8 represent the flux of H_2 that is lost in the short-circuit, the electrons being used to reduce the incoming O_2. The stoichiometry of the reaction imposes that $(s^\infty - s_{app}^\infty)/(1 - \xi_f)$ is proportional to $o^\infty/(1 - \xi_m)$ (they would be equal if $D_S = D_O$). The fact that the reduction of O_2 is limited by the transport of O_2 and electrons in the outer layer imposes that $1 - \xi_m$ and $1 - \xi_f$ are proportional to one another (eq 17), which leads to s_{app}^∞ being constant.

The expression of the steady-state current under aerobic conditions (horizontal lines in Figure 9 and eq 26) is surprisingly simple:

$$J/F = (D_S S^\infty - D_O O^\infty)/l \tag{28a}$$

$$\frac{J}{J_0} = \frac{D_S S^\infty - D_O O^\infty}{D_S S^\infty + D_A A^\Sigma} \tag{28b}$$

where J_0 is the current observed in the absence of O_2, defined in eq 9. Equation 28a gives a condition for the protection mechanism to be operational: $D_S S^\infty > D_O O^\infty$. If this condition is not fulfilled, the flux of electrons that results from H_2 oxidation at ξ_f is not sufficient to reduce the incoming O_2 at ξ_m, the concentration of H_2 in the film drops down to zero, and the film quickly inactivates (not shown).

There have been reports about the oxygen tolerance of hydrogenase that results from its immobilization into thin viologen films or in planar tethered bilayer membranes containing a quinone mediator.[3,15] In these cases the protection mechanism seems to result from reductive reactivation by the mediators or adjacent hydrogenase molecules. In the case that we considered, the film can protect the enzyme even if the inactivation is irreversible (k_r can be zero), and the value of the rate constant for the inhibition reaction k_i does not determine the resistance to O_2 either. (Note that things would be different if k_i was so small that the reduction of O_2 in the outer layer was limited by the reaction rather than transport, or if k_r was so large that a steady-state was reached under aerobic conditions.) The observation that the exact values of k_r and k_i do not really matter implies that the strategy for improving the resistance of the enzyme/film is entirely distinct from the situation where the catalysts is a submonolayer of enzyme that undergoes direct electron transfer with the electrode. In the latter case, it has been clearly established that the resistance to O_2 of certain [NiFe]-hydrogenases is the consequence of their rate of reactivation being large,[25,27,61] and this has guided the use of protein engineering to design O_2-tolerant [NiFe]-hydrogenases in a rational manner.[29,30] Regarding [FeFe]-hydrogenases, which do not reactivate after exposure to O_2, theoretical studies have been used to propose mutations that may decrease the rate of reaction with O_2.[51,62] From the analysis above, it appears that *under the conditions we considered*, the rate of reactivation and the rate of inactivation of the enzyme do not determine the resistance of the enzyme-film. This suggests that enzymes that inactivate very quickly in the presence of O_2 and/or reactivate very slowly under reducing conditions may also be protected by polymer films, consistent with the (unpublished) observation of ours that [FeFe]-hydrogenases and [NiFe]-hydrogenases give similar results after incorporation in a polymer film.

Nonbiological scaffolds (polymers, metal−organic frameworks, and other porous materials) can also be used for embedding and protecting fragile synthetic catalysts (reviewed in ref 63). Considering the protection mechanism described in this paper and initially suggested in ref 35, it should now be possible to reconsider libraries of molecular and biocatalysts that have been dismissed for applications due to insufficient stability. Further optimization of the hydrogel properties and its extension to other catalysts for other reactions will require an in-depth quantitative understanding of the electron transfer, mass transport, and catalysis within the hydrogel. We hope that this paper sets the grounds for such studies.

It may be tempting to speculate about the general biological relevance of the above protection mechanism, considering the observation that hydrogenases are protected against O_2 when embedded into a tethered bilayer.[3] However, a crucial and

DOI: 10.1021/jacs.5b01194
J. Am. Chem. Soc. 2015, 137, 5494−5505

unique feature of the system we investigate, which has no correspondence in vivo, is the spatial separation within the depth of the film between the enzyme that gives electrons to the electrode and the enzyme that produces the electrons that quench dioxygen.

■ ASSOCIATED CONTENT

Supporting Information

Two-dimensional case diagram; AFM image of a thin film of viologen polymer in an IDA electrode; dependence of the peak current on scan rate, regarding the slow scan CV experiments in Figure 2A, and the estimation of D_A; fast scan CV experiments; chronoamperometry experiments; differential equations; concentration profiles; list of symbols. This material is available free of charge via the Internet at http://pubs.acs.org.

■ AUTHOR INFORMATION

Corresponding Authors

*nicolas.plumere@rub.de

*christophe.leger@imm.cnrs.fr

Notes

The authors declare no competing financial interest.

■ ACKNOWLEDGMENTS

The authors thank Alaa Alsheikh Oughli for helping with the experiments in Mülheim. The work in France was funded by the CNRS, Aix-Marseille University, Agence Nationale de la Recherche (ANR-12-BS08-0014, ANR-14-CE05-0010), Région Provence Alpes Côte d'Azur (PACA), and supported by the "Pôle de compétitivité Capénergies". The French authors are part of FrenchBIC (www.frenchbic.cnrs.fr). The work in Bochum and Mülheim was supported by the Deutsch-Israelische Projektkooperation (DIP) in the framework of the project "Nanoengineered optoelectronics with biomaterials and bioinspired assemblies" and by the Cluster of Excellence RESOLV (EXC 1069) funded by the Deutsche Forschungsgemeinschaft (DFG). H.L. is grateful for the support by the China Scholarship Council (CSC). O.R. and W.L. acknowledge funding from the Max Planck Society.

■ REFERENCES

(1) Hambourger, M.; Gervaldo, M.; Svedruzic, D.; King, P. W.; Gust, D.; Ghirardi, M.; Moore, A. L.; Moore, T. A. *J. Am. Chem. Soc.* **2008**, *130*, 2015−2022.

(2) Caputo, C. A.; Gross, M. A.; Lau, V. W.; Cavazza, C.; Lotsch, B. V.; Reisner, E. *Angew. Chem., Int. Ed.* **2014**, *53*, 11538−11542.

(3) Radu, V.; Frielingsdorf, S.; Evans, S. D.; Lenz, O.; Jeuken, L. J. C. *J. Am. Chem. Soc.* **2014**, *136*, 8512−8515.

(4) Gutiérrez-Sanz, O.; Tapia, C.; Marques, M. C.; Zacarias, S.; Vélez, M.; Pereira, I. A.; de Lacey, A. L. *Angew. Chem., Int. Ed.* **2015**, *54*, 2684−2687.

(5) de Poulpiquet, A.; Ranava, D.; Monsalve, K.; Giudici-Orticoni, M.-T.; Lojou, E. *ChemElectroChem.* **2014**, *1*, 1724−1750.

(6) Krishnan, S.; Armstrong, F. A. *Chem. Sci.* **2012**, *3*, 1015−1023.

(7) Brown, K. A.; Song, Q.; Mulder, D. W.; King, P. W. *ACS Nano* **2014**, *8*, 10790−10798.

(8) Rüdiger, O.; Abad, J. M.; Hatchikian, E. C.; Fernandez, V. M.; de Lacey, A. L. *J. Am. Chem. Soc.* **2005**, *127*, 16008−16009.

(9) Baffert, C.; Bertini, L.; Lautier, T.; Greco, C.; Sybirna, K.; Ezanno, P.; Etienne, E.; Soucaille, P; Bertrand, P.; Bottin, H.; Meynial-Salles, I.; De Gioia, L.; Léger, C. *J. Am. Chem. Soc.* **2011**, *133*, 2096−2099.

(10) McIntosh, C. L.; Germer, F.; Schulz, R.; Appel, J.; Jones, A. K. *J. Am. Chem. Soc.* **2011**, *133*, 11308−11319.

(11) Utesch, T.; Millo, D.; Castro, M. A. A.; Hildebrandt, P.; Zebger, I.; Mroginski, M. A. A. *Langmuir* **2013**, *29*, 673−682.

(12) Bediako, D. K.; Costentin, C.; Jones, E. C.; Nocera, D. G.; Savéant, J.-M. *J. Am. Chem. Soc.* **2013**, *135*, 10492−10502.

(13) le Goff, A.; Artero, V.; Jousselme, B.; Tran, P. D. D.; Guillet, N.; Métayé, R.; Fihri, A.; Palacin, S.; Fontecave, M. *Science* **2009**, *326*, 1384−1387.

(14) Ciaccafava, A.; Infossi, P.; Giudici-Orticoni, M.-T.; Lojou, E. *Langmuir* **2010**, *26*, 18534−18541.

(15) Morozov, S. V.; Voronin, O. G.; Karyakin, E. E.; Zorin, N. A.; Cosnier, S.; Karyakin, A. A. *Electrochem. Commun.* **2006**, *8*, 851−854.

(16) Baur, J.; Le Goff, A.; Dementin, S.; Holzinger, M.; Rousset, M.; Cosnier, S. *Int. J. Hydrogen Energy* **2011**, *36*, 12096−12101.

(17) Karyakin, A. A.; Morozov, S. V.; Voronin, O. G.; Zorin, N. A.; Karyakina, E. E.; Fateyev, V. N.; Cosnier, S. *Angew. Chem., Int. Ed.* **2007**, *46*, 7244−7246.

(18) Abou Hamdan, A.; Burlat, B.; Gutiérrez-Sanz, O.; Liebgott, P.; Baffert, C.; de Lacey, A.; Rousset, M.; Guigliarelli, B.; Léger, C.; Dementin, S. *Nat. Chem. Biol.* **2013**, *9*, 15−17.

(19) Stripp, S. T.; Goldet, G.; Brandmayr, C.; Sanganas, O.; Vincent, K. A.; Haumann, M.; Armstrong, F. A.; Happe, T. *Proc. Natl. Acad. Sci. U.S.A.* **2009**, *106*, 17331−17336.

(20) Swanson, K. D.; Ratzloff, M. W.; Mulder, D. W.; Artz, J. H.; Ghose, S.; Hoffman, A.; White, S.; Zadvornyy, O. A.; Broderick, J. B.; Bothner, B.; King, P. W.; Peters, J. W. *J. Am. Chem. Soc.* **2015**, *137*, 1809−1816.

(21) Shomura, Y.; Yoon, K.-S. S.; Nishihara, H.; Higuchi, Y. *Nature* **2011**, *479*, 253−256.

(22) Fritsch, J.; Scheerer, P.; Frielingsdorf, S.; Kroschinsky, S.; Friedrich, B.; Lenz, O.; Spahn, C. M. *Nature* **2011**, *479*, 249−252.

(23) Volbeda, A.; Darnault, C.; Parkin, A.; Sargent, F.; Armstrong, F. A.; Fontecilla-Camps, J. C. *Structure* **2013**, *21*, 184−190.

(24) Wulff, P.; Day, C. C.; Sargent, F.; Armstrong, F. A. *Proc. Natl. Acad. Sci. U.S.A.* **2014**, *111*, 6606−6611.

(25) Cracknell, J. A.; Wait, A. F.; Lenz, O.; Friedrich, B.; Armstrong, F. A. *Proc. Natl. Acad. Sci. U.S.A.* **2009**, *106*, 20681−20686.

(26) Fourmond, V.; Infossi, P.; Giudici-Orticoni, M.-T.; Bertrand, P.; Léger, C. J. *Am. Chem. Soc.* **2010**, *132*, 4848−4857.

(27) Pandelia, M.-E.; Fourmond, V.; Tron-Infossi, P.; Lojou, E.; Bertrand, P.; Léger, C.; Giudici-Orticoni, M.-T.; Lubitz, W. *J. Am. Chem. Soc.* **2010**, *132*, 6991−7004.

(28) Pandelia, M.-E.; Bykov, D.; Izsak, R.; Infossi, P.; Giudici-Orticoni, M.-T.; Bill, E.; Neese, F.; Lubitz, W. *Proc. Natl. Acad. Sci. U.S.A.* **2013**, *110*, 483−488.

(29) Liebgott, P.-P.; de Lacey, A. L.; Burlat, B.; Cournac, L.; Richaud, P.; Brugna, M.; Fernandez, V. M.; Guigliarelli, B.; Rousset, M.; Léger, C.; Dementin, S. *J. Am. Chem. Soc.* **2011**, *133*, 986−997.

(30) Abou Hamdan, A.; Liebgott, P.-P.; Fourmond, V.; Gutiérrez-Sanz, O.; de Lacey, A. L.; Infossi, P.; Rousset, M.; Dementin, S.; Léger, C. *Proc. Natl. Acad. Sci. U.S.A.* **2012**, *109*, 19916−19921.

(31) Lakadamyali, F.; Kato, M.; Muresan, N. M.; Reisner, E. *Angew. Chem., Int. Ed.* **2012**, *51*, 9381−9384.

(32) Wakerley, D. W.; Gross, M. A.; Reisner, E. *Chem. Commun.* **2014**, *50*, 15995−15998.

(33) Kleingardner, J. G.; Kandemir, B.; Bren, K. L. *J. Am. Chem. Soc.* **2014**, *136*, 4−7.

(34) Dey, S.; Rana, A.; Crouthers, D.; Mondal, B.; Das, P. K.; Darensbourg, M. Y.; Dey, A. *J. Am. Chem. Soc.* **2014**, *136*, 8847−8850.

(35) Plumeré, N.; Rüdiger, O.; Oughli, A. A.; Williams, R.; Vivekananthan, J.; Pöller, S.; Schuhmann, W.; Lubitz, W. *Nat. Chem.* **2014**, *6*, 822−827.

(36) Ogata, H.; Nishikawa, K.; Lubitz, W. *Nature*. **2015**, DOI: 10.1038/nature14110.

(37) Fichtner, C.; Laurich, C.; Bothe, E.; Lubitz, W. *Biochemistry* **2006**, *45*, 9706−9716.

(38) Yagi, T.; Kimura, K.; Daidoji, H.; Sakai, F.; Tamura, S.; Inokuchi, H. *J. Biochem.* **1976**, *79*, 661−671.

(39) Plumeré, N.; Henig, J.; Campbell, W. H. *Anal. Chem.* **2012**, *84*, 2141−2146.

DOI: 10.1021/jacs.5b01194
J. Am. Chem. Soc. 2015, 137, 5494−5505

(40) Swoboda, M.; Henig, J.; Cheng, H.-M.; Brugger, D.; Haltrich, D.; Plumeré, N.; Schlierf, M. *ACS Nano* **2012**, *6*, 6364−6369.
(41) Fourmond, V.; Hoke, K.; Heering, H. A.; Baffert, C.; Leroux, F.; Bertrand, P.; Léger, C. *Bioelectrochem.* **2009**, *76*, 141−147.
(42) Bartlett, P. N.; Pratt, K. F. E. *J. Electroanal. Chem.* **1995**, *397*, 61−78.
(43) Saveant, J. M. *Elements of molecular and biomolecular electrochemistry*; John Willey & sons, Inc.: Hoboken, NJ, 2006.
(44) Flexer, V.; Calvo, E. J.; Bartlett, P. N. *J. Electroanal. Chem.* **2010**, *646*, 24−32.
(45) Andrieux, C. P.; Dumas-Bouchiat, J. M.; Savéant, J. M. *J. Electroanal. Chem. Interfacial Electrochem.* **1984**, *169*, 9−21.
(46) Chidsey, C. E.; Feldman, B. J.; Lundgren, C.; Murray, R. W. *Anal. Chem.* **1986**, *58*, 601−607.
(47) Mao, F.; Mano, N.; Heller, A. *J. Am. Chem. Soc.* **2003**, *125*, 4951−4957.
(48) Bard, A. J.; Faulkner, L. R. *Electrochemical Methods. Fundamental and Applications*, 3rd ed.; John Wiley & Sons, Inc.: New York, 2004.
(49) Chakraborty, D.; McClellan, E.; Hasselbeck, R.; Barton, S. C. *J. Electrochem. Soc.* **2014**, *161*, H3076−H3082.
(50) Léger, C.; Dementin, S.; Bertrand, P.; Rousset, M.; Guigliarelli, B. *J. Am. Chem. Soc.* **2004**, *126*, 12162−12172.
(51) Greco, C.; Fourmond, V.; Baffert, C.; Wang, P.-h.; Dementin, S.; Bertrand, P.; Bruschi, M.; Blumberger, J.; de Gioia, L.; Léger, C. *Energy Environ. Sci.* **2014**, *7*, 3543−3573.
(52) Jähne, B.; Heinz, G.; Dietrich, W. *J. Geophys. Res.* **1987**, *92*, 10767−10776.
(53) *CRC Handbook of Chemistry and Physics: A Ready-Reference Book of Chemical and Physical Data*, 88th ed.; CRC Press.: Boca Raton, FL, 2008; Vol. *6*.
(54) Dementin, S.; Belle, V.; Bertrand, P.; Guigliarelli, B.; Adryanczyk-Perrier, G.; de Lacey, A.; Fernandez, V. M.; Rousset, M.; Léger, C. *J. Am. Chem. Soc.* **2006**, *128*, 5209−5218.
(55) de Lacey, A. L.; Hatchikian, E. C.; Volbeda, A.; Frey, M.; Fontecilla-Camps, J. C.; Fernandez, V. M. *J. Am. Chem. Soc.* **1997**, *119*, 7181−7189.
(56) Thorneley, R. N. F. *Biochim. Biophys. Acta* **1974**, *333*, 487−496.
(57) *NIST Handbook of Mathematical Functions*; Olver, Frank W. J., Lozier, D. W., Boisvert, R. F., Clark, C. W., Eds.; Cambridge University Press: Cambridge, 2010, (http://dlmf.nist.gov/).
(58) Kothe, T.; Pöller, S.; Zhao, F.; Fortgang, P.; Rögner, M.; Schuhmann, W.; Plumeré, N. *Chem.—Eur. J.* **2014**, *20*, 11029−11034.
(59) Terrill, R. H.; Hutchison, J. E.; Murray, R. W. *J. Phys. Chem. B* **1997**, *101*, 1535−1542.
(60) Gallaway, J. W.; Calabrese Barton, S. A. *J. Am. Chem. Soc.* **2008**, *130*, 8527−8536.
(61) Xu, L.; Armstrong, F. A. *RSC Adv.* **2015**, *5*, 3649−3656.
(62) Kubas, A.; De Sancho, D.; Best, R. B.; Blumberger, J. *Angew. Chem., Int. Ed.* **2014**, *53*, 4081−4084.
(63) Caserta, G.; Roy, S.; Atta, M.; Artero, V.; Fontecave, M. *Curr. Opin. Chem. Biol.* **2015**, *25*, 36−47.

DOI: 10.1021/jacs.5b01194
J. Am. Chem. Soc. 2015, 137, 5494−5505